Asian Journal of Chemistry; Vol. 27, No. 1 (2015), 277-281

ASIAN JOURNAL OF CHEMISTRY

http://dx.doi.org/10.14233/ajchem.2015.17405

Cyclic Microwave-Assisted Sol-Gel Process of $SrGd_2(MoO_4)_4:Er^{3+}/Yb^{3+}$ Phosphors and Their Upconversion Mechanisms by Two-Photon Process

CHANG SUNG LIM

Department of Advanced Materials Science and Engineering, Hanseo University, Seosan 356-706, Republic of Korea

Corresponding author: Tel./Fax: +82 41 6601445; E-mail: cslim@hanseo.ac.kr

Received: 17 February 2014; *Accepted*: 8 May 2014; *Published online*: 26 December 2014; AJC-16555

$SrGd_2(MoO_4)_4:Er^{3+}/Yb^{3+}$ green phosphors with doping concentrations of Er^{3+} and Yb^{3+} have been successfully synthesized by a cyclic microwave-assisted sol-gel method and the upconversion mechanisms by a two-photon process have been investigated. Well-crystallized particles, formed after heat-treatment at 900 °C for 12 h, showed a fine and homogeneous morphology with particle sizes of 2-5 μm. Under excitation at 980 nm, $SrGd_2(MoO_4)_4:Er^{3+}/Yb^{3+}$ particles exhibited strong 525 and 550-nm emission bands in the green region correspond to the $^2H_{11/2} \rightarrow {}^4I_{15/2}$ and $^4S_{3/2} \rightarrow {}^4I_{15/2}$ transitions, respectively, while the very weak 655 nm emission band in the red region corresponds to the $^4F_{9/2} \rightarrow {}^4I_{15/2}$ transition. The Raman spectra of the particles indicated the presence of strong peaks at both higher frequencies (1023, 1092 and 1325 cm^{-1}) and at lower frequencies (233, 293, 365, 428, 538 and 594 cm^{-1}).

Keywords: Green phosphor, Sol-gel, Upconversion, Two-photon process.

INTRODUCTION

Upconversion photoluminescence particles can convert near infrared radiation of low energy into visible radiation of high energy. Recently, these upconversion photoluminescence particles have evolved in their applications, showing great potential for imaging and biodetection assays in both *in vitro* and *in vivo* with their high penetration depth into tissues, sharp emission bands and high resistance to photobleaching, which overcome the current limitations in traditional photoluminescence materials[1-3]. The double molybdate compounds of $MR_2(MoO_4)_4$ (M: bivalent alkaline earth metal ion, R: trivalent rare earth ion) belong to a group of double alkaline earth lanthanide molybdates. With the decrease in the ionic radius of alkaline earth metal ions ($R_{Ca} < R_{Sr} < R_{Ba}$; R = ionic radius), the structure of $MR_2(MoO_4)_4$ could be transformed to a highly disordered tetragonal Scheelite structure from the monoclinic structure. It is possible that that the trivalent rare earth ions in the disordered tetragonal-phase could be partially substituted by Er^{3+} and Yb^{3+} ions and the ions are effectively doped into the crystal lattices of the tetragonal phase due to the similar radii of trivalent rare earth ions of R^{3+}, resulted in the excellent upconversion photoluminescence properties[4-6]. Among the rare earth ions, the Er^{3+} ion is suitable for converting infrared to visible light through the upconversion process due to proper electronic energy level configuration. The co-doped Yb^{3+} ion and Er^{3+} ion can remarkably enhance the upconversion efficiency from infrared to visible light due to the efficiency energy transfer from Yb^{3+} to Er^{3+}. The Yb^{3+} ion as a sensitizer can be effectively excited by incident light source energy that is transferred to the activator, from which radiation can be emitted. The Er^{3+} ion activator is the luminescence center of the upconversion particles, while the sensitizer enhances the upconversion luminescence efficiency[7-9].

Recently, rare earth activated $MR_2(MoO_4)_4$ (M = Ba, Sr, Ca; R = La, Gd, Y) have attracted great attention because of their spectroscopic characteristics with excellent upconversion photoluminescence properties. Several processes have been developed to prepare the rare-earth-doped double molybdates, including solid-state reactions[10-14], co-precipitation[15,16], sol-gel method[4-6], hydrothermal method[17,18], Pechini method[19,20], organic gel-thermal decomposition[21] and microwave-assisted hydrothermal method[22]. For practical applications of upconversion phosphors in products, well defined features such as homogeneous particle size distribution and morphology are required. Usually, double molybdates are prepared by a solid-state method that requires long mixing time, subsequent grinding and high temperatures, which results in loss of the emission intensity. Sol-gel process has some advantages including good homogeneity, low calcination temperature, small particle size and narrow particle size distribution. However, the sol-gel process has a disadvantage in that it takes a long time for gelation. As compared with the usual methods, microwave synthesis has advantages of very short reaction time with the homogeneous

morphology features for high purity of final polycrystalline. Microwave heating is delivered to the material surface by radiant and/or convection heating, which is transferred to the bulk of the material *via* conduction[23,24]. A cyclic microwave-assisted sol-gel process is a cost-effective method that provides high-quality luminescent materials with easy scale-up in short time periods. However, the cyclic microwave-assisted sol-gel process has not been reported.

In this study, $SrGd_2(MoO_4)_4:Er^{3+}/Yb^{3+}$ phosphors with the doping concentrations of Er^{3+} and Yb^{3+} (Er^{3+} = 0.05, 0.1, 0.2 and Yb^{3+} = 0.2, 0.45) were synthesized by a cyclic microwave-assisted sol-gel method for the first time. The synthesized $SrGd_2(MoO_4)_4:Er^{3+}/Yb^{3+}$ particles were characterized by X-ray diffraction (XRD), scanning electron microscopy (SEM) and energy-dispersive X-ray spectroscopy (EDS). The optical properties were examined comparatively using photoluminescence (PL) emission and Raman spectroscopy.

EXPERIMENTAL

Appropriate stoichiometric amounts of $Sr(NO_3)_2$ (99 %, Sigma-Aldrich, USA), $Gd(NO_3)_3·6H_2O$ (99 %, Sigma-Aldrich, USA), $(NH_4)_6Mo_7O_{24}·4H_2O$ (99 %, Alfa Aesar, USA), $Er(NO_3)_3·5H_2O$ (99.9 %, Sigma-Aldrich, USA), $Yb(NO_3)_3·5H_2O$ (99.9 %, Sigma-Aldrich, USA), citric acid (99.5 %, Daejung Chemicals, Korea), NH_4OH (A.R.), ethylene glycol (A.R.) and distilled water were used to prepare $SrGd_2(MoO_4)_4$, $SrGd_{1.8}(MoO_4)_4:Er_{0.2}$, $SrGd_{1.7}(MoO_4)_4:Er_{0.1}Yb_{0.2}$ and $SrGd_{1.5}(MoO_4)_4:Er_{0.05}Yb_{0.45}$ compounds. To prepare $SrGd_2(MoO_4)_4$, 0.4 mol % $Sr(NO_3)_2$ and 0.4 mol % $(NH_4)_6Mo_7O_{24}·4H_2O$ were dissolved in 20 mL of ethylene glycol and 80 mL of 5M NH_4OH under vigorous stirring and heating. Subsequently, 0.8 mol % $Gd(NO_3)_3·6H_2O$ and citric acid (with a molar ratio of citric acid to total metal ions of 2:1) were dissolved in 100 mL of distilled water under vigorous stirring and heating. Then, the solutions were mixed together under vigorous stirring and heating. At the end, the highly transparent solutions were obtained and adjusted to pH = 7-8 by the addition of NH_4OH or citric acid. In the second way, to prepare $SrGd_{1.8}(MoO_4)_4:Er_{0.2}$, the mixture of 0.72 mol % $Gd(NO_3)_3·6H_2O$ with 0.08 mol % $Er(NO_3)_3·5H_2O$ was used for creation of the rare earth solution. In the third way, to prepare $SrGd_{1.7}(MoO_4)_4:Er_{0.1}Yb_{0.2}$, the mixture of 0.68 mol % $Gd(NO_3)_3·6H_2O$ with 0.04 mol % $Er(NO_3)_3·5H_2O$ and 0.08 mol % $Yb(NO_3)_3·5H_2O$ was used for creation of the rare earth solution. In the fourth way, to prepare $SrGd_{1.5}(MoO_4)_4:Er_{0.05}Yb_{0.45}$, the rare earth containing solution was generated using 0.6 mol % $Gd(NO_3)_3·6H_2O$ with 0.02 mol % $Er(NO_3)_3·5H_2O$ and 0.18 mol % $Yb(NO_3)_3·5H_2O$.

The transparent solutions were placed into a microwave oven operating at a frequency of 2.45 GHz with a maximum output-power of 1250 W for 0.5 h. The working cycle of the microwave reaction was controlled precisely between 40 s on and 20 s off for 15 min, followed by further treatment of 30 s on and 30 s off for 15 min. The samples were treated with ultrasonic radiation for 10 min to produce a light yellow transparent sol. After this stage, the light yellow transparent sols were dried at 120 °C in a dry oven for 48 h to obtain black dried gels. The black dried gels were grinded and heat-treated at 900 °C for 12 h with 100 °C interval between 600-900 °C. Finally, the white particles were obtained for $SrGd_2(MoO_4)_4$ with pink particles for the doped compositions.

The phase composition of the synthesized particles was identified using XRD (D/MAX 2200, Rigaku, Japan). The microstructure and surface morphology were observed using SEM/EDS (JSM-5600, JEOL, Japan). The photoluminescence spectra were recorded using a spectrophotometer (Perkin Elmer LS55, UK) at room temperature. Raman spectroscopy measurements were performed using a LabRam Aramis (Horiba Jobin-Yvon, France). The 514.5-nm line of an Ar ion laser was used as an excitation source and the power on the samples was kept at 0.5 mW.

RESULTS AND DISCUSSION

Fig. 1 shows the XRD patterns of the (a) JCPDS 08-0482 data of $SrMoO_4$, the synthesized (b) $SrGd_2(MoO_4)_4$, (c) $SrGd_{1.8}(MoO_4)_4:Er_{0.2}$, (d) $SrGd_{1.7}(MoO_4)_4:Er_{0.1}Yb_{0.2}$ and (e) $SrGd_{1.5}(MoO_4)_4:Er_{0.05}Yb_{0.45}$ particles. All of the XRD peaks could be assigned to the tetragonal-phase $SrMoO_4$ with a Scheelite-type structure of space group $I4_{1/a}$ with lattice parameters of a = b = 5.3796 Å and c = 11.9897 Å[23-25], which was in good agreement with the crystallographic data of $SrMoO_4$ (JCPDS 08-0482). This means that the tetragonal-phase of $SrGd_2(MoO_4)_4:Er^{3+}/Yb^{3+}$ can be prepared using the cyclic microwave-assisted sol-gel method. This suggests that the cyclic microwave-assisted sol-gel route is suitable for the growth of $SrGd_2(MoO_4)_4:Er^{3+}/Yb^{3+}$ crystallites and for developing the strongest intensity peaks at the (112), (204) and (312) planes, which are the major peaks of $SrMoO_4$[23-25]. Impurity phases were detected at 25° and 31.5° in Fig. 1(d) and at 24°, 25°, 25.5°, 29.5° and 32° in Fig. 2(e). The foreign reflexes are marked with asterisk in Fig. 1(d) when the doping concentration of Er^{3+}/Yb^{3+} is 0.04/008 mol % and in Fig. 1(e) when the doping concentration of Er^{3+}/Yb^{3+} is 0.02/0.18 mol %. However, it is difficult to identify the impurity phases since very weak peaks are observed. The similar impurity phase was also observed in the case of Er^{3+}/Yb^{3+} doped $SrMoO_4$ phosphor when the doping concentration of Er^{3+}/Yb^{3+} is 0.02/0.18 mol %[26]. Post heat-treatment plays an important role in a well-defined crystallized morphology. To achieve a well-defined crystalline morphology, the $SrGd_2(MoO_4)4:Er^{3+}/Yb^{3+}$ phases need to be heat treated at 900 °C for 12 h. It is assumed that the doping amount of Er^{3+}/Yb^{3+} has a great effect on the crystalline cell volume of the $SrGd_2(MoO_4)_4$, because of the different ionic sizes and energy band gaps. This means that the obtained samples have a tetragonal-phase after partial substitution of Gd^{3+} by Er^{3+} and Yb^{3+} ions and the ions are effectively doped into crystal lattices of the $SrGd_2(MoO_4)_4$ phase due to the similar radii of Gd^{3+}, Er^{3+} and Yb^{3+} [4-6].

Fig. 2 shows SEM images of the synthesized $SrGd_{1.5}(MoO_4)_4:Er_{0.05}Yb_{0.45}$ particles. The as-synthesized sample is well crystallized with a fine and homogeneous morphology and particle size of 2-5 μm. The combination of doping amounts of 0.02 mol % Er^{3+} and 0.18 mol % Yb^{3+} for $SrGd_{1.5}(MoO_4)_4:Er_{0.05}Yb_{0.45}$ has a great effect on the morphological features. Fig. 3 shows the energy-dispersive X-ray spectroscopy patterns of the synthesized (a) $SrGd_{1.8}(MoO_4)_4:Er_{0.2}$ and (b) $SrGd_{1.5}(MoO_4)_4:Er_{0.05}Yb_{0.45}$ particles and quantitative compo-

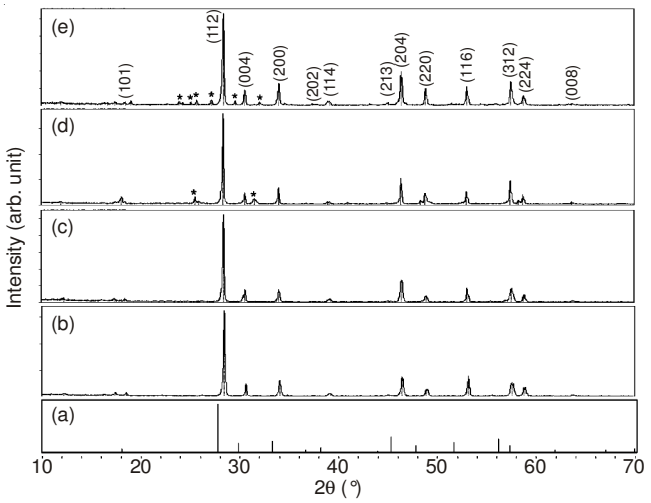

Fig. 1. X-ray diffraction patterns of the (a) JCPDS 08-0482 data of $SrMoO_4$, the synthesized (b) $SrGd_2(MoO_4)_4$, (c) $SrGd_{1.8}(MoO_4)_4:Er_{0.2}$, (d) $SrGd_{1.7}(MoO_4)_4:Er_{0.1}Yb_{0.2}$ and (e) $SrGd_{1.5}(MoO_4)_4:Er_{0.05}Yb_{0.45}$ particles

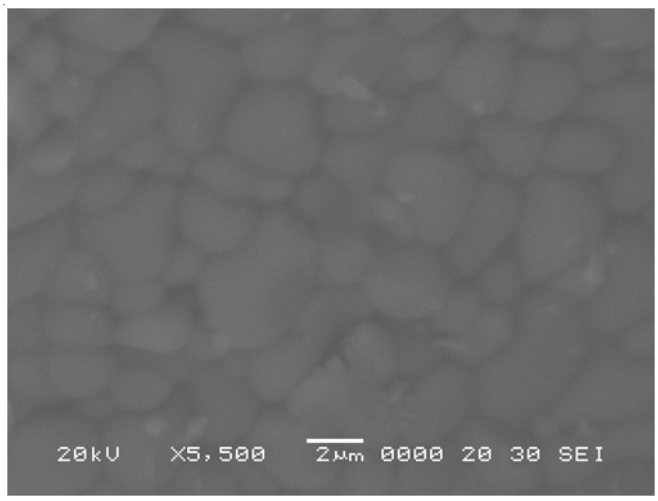

Fig. 2. Scanning electron microscopy images of the synthesized $SrGd_{1.5}(MoO_4)_4:Er_{0.05}Yb_{0.45}$ particles

sitions of (c) $SrGd_{1.8}(MoO_4)_4:Er_{0.2}$ and (d) $SrGd_{1.5}$-$(MoO_4)_4:Er_{0.05}Yb_{0.45}$ particles. The EDS pattern shows that the (a) $SrGd_{1.8}(MoO_4)_4:Er_{0.2}$ and (b) $SrGd_{1.5}(MoO_4)_4:Er_{0.05}Yb_{0.45}$ particles are composed of Sr, Gd, Mo, O and Er for $SrGd_2(MoO_4)_4:Er^{3+}$ and Sr, Gd, Mo, O, Er and Yb for $SrGd_{1.5}(MoO_4)_4:Er_{0.05}Yb_{0.45}$ particles. The quantitative compositions (c) and (d) are in good relation with nominal compositions of the $SrGd_{1.8}(MoO_4)_4:Er_{0.2}$ and $SrGd_{1.5}(MoO_4)_4:Er_{0.05}Yb_{0.45}$ particles. The relation of Sr, Gd, Mo, O, Er and Yb components exhibits that $SrGd_{1.8}(MoO_4)_4:Er_{0.2}$ and $SrGd_{1.5}(MoO_4)_4:Er_{0.05}Yb_{0.45}$ particles can be successfully synthesized using the cyclic microwave-assisted sol-gel method. The cyclic microwave-assisted sol-gel process of double molybdates provides the energy to synthesize the bulk of the material uniformly, so that fine particles with controlled morphology can be fabricated in short time periods. The method is a cost-effective way to provide highly homogeneous products with easy scale-up and is a viable alternative for the rapid synthesis of upconversion particles.

Fig. 4 shows the upconversion photoluminescence emission spectra of the as-prepared (a) $SrGd_2(MoO_4)_4$, (b) $SrGd_{1.8}(MoO_4)_4:Er_{0.2}$, (c) $SrGd_{1.7}(MoO_4)_4:Er_{0.1}Yb_{0.2}$ and (d)

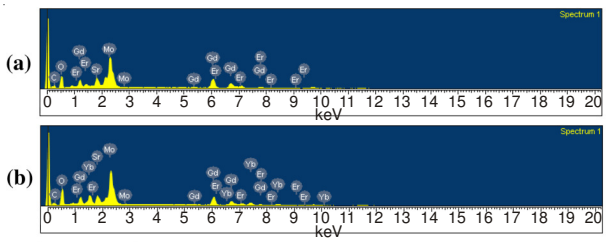

(c)

Spectrum	In stats.	C	O	Sr	Mo	Gd	Er	Total
Spectrum 1	Yes	12.75	33.34	5.55	26.71	19.60	2.05	100.00
Spectrum 2	Yes	13.41	32.78	5.30	26.57	19.00	2.95	100.00
Spectrum 3	Yes	11.76	33.20	5.29	27.30	19.60	2.85	100.00
Spectrum 4	Yes	11.03	33.39	5.30	27.63	20.24	2.42	100.00
Spectrum 5	Yes	11.61	33.23	5.08	27.85	19.65	2.58	100.00
Mean		12.11	33.18	5.31	27.21	19.62	2.57	100.00
Std. deviation		0.95	0.24	0.17	0.56	0.44	0.36	
Max.		13.41	33.39	5.55	27.85	20.24	2.95	
Min.		11.03	32.78	5.08	26.57	19.00	2.05	

(d)

Spectrum	In stats.	C	O	Sr	Mo	Gd	Er	Yb	Total
Spectrum 1	Yes	7.55	37.71	4.77	26.76	15.26	0.62	7.31	100.00
Spectrum 2	Yes	4.66	39.08	4.79	28.23	15.41	0.48	7.34	100.00
Spectrum 3	Yes	2.38	39.52	5.23	28.54	16.06	0.95	7.32	100.00
Spectrum 4	Yes	7.74	37.45	4.54	27.29	15.17	0.63	7.18	100.00
Spectrum 5	Yes	7.69	37.67	4.63	27.08	14.93	0.62	7.39	100.00
Mean		6.01	38.29	4.79	27.58	15.37	0.66	7.31	100.00
Std. deviation		2.40	0.94	0.27	0.76	0.43	0.17	0.08	
Max.		7.74	39.52	5.23	28.54	16.06	0.95	7.39	
Min.		2.38	37.45	4.54	26.76	14.93	0.48	7.18	

Fig. 3. Energy-dispersive X-ray spectroscopy patterns of the synthesized (a) $SrGd_{1.8}(MoO_4)_4:Er_{0.2}$ and (b) $SrGd_{1.5}(MoO_4)_4:Er_{0.05}Yb_{0.45}$ particles and quantitative compositions of (c) $SrGd_{1.8}(MoO_4)_4:Er_{0.2}$ and (d) $SrGd_{1.5}(MoO_4)_4:Er_{0.05}Yb_{0.45}$ particles

$SrGd_{1.5}(MoO_4)_4:Er_{0.05}Yb_{0.45}$ particles excited under 980 nm at room temperature. $SrGd_{1.7}(MoO_4)_4:Er_{0.1}Yb_{0.2}$ and $SrGd_{1.5}(MoO_4)_4:Er_{0.05}Yb_{0.45}$ particles exhibit strong 525 and 550 nm emission bands in the green region correspond to the $^2H_{11/2} \rightarrow {}^4I_{15/2}$ and $^4S_{3/2} \rightarrow {}^4I_{15/2}$ transitions, respectively, while the very weak 655 nm emission band in the red region corresponds to the $^4F_{9/2} \rightarrow {}^4I_{15/2}$ transition. The upconversion intensities of (a) $SrGd_2(MoO_4)_4$ and (b) $SrGd_{1.8}(MoO_4)_4:Er_{0.2}$ have not being detected. The upconversion intensity of (d) $SrGd_{1.5}(MoO_4)_4:Er_{0.05}Yb_{0.45}$ is much higher than that of (c) $SrGd_{1.7}(MoO_4)_4:Er_{0.1}Yb_{0.2}$ particles. Similar results are also observed from Er^{3+}/Yb^{3+} co-doped in other host matrices, which are assigned in the upconversion emission spectra with the green emission intensity ($^2H_{11/2} \rightarrow {}^4I_{15/2}$ and $^4S_{3/2} \rightarrow {}^4I_{15/2}$ transitions) and the red emission intensity ($^4F_{9/2} \rightarrow {}^4I_{15/2}$ transition)[7,10,18,27].

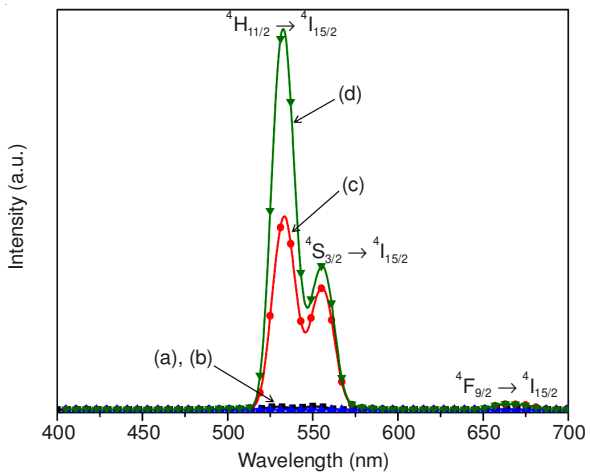

Fig. 4. Upconversion photoluminescence emission spectra of (a) $SrGd_2(MoO_4)_4$, (b) $SrGd_{1.8}(MoO_4)_4:Er_{0.2}$, (c) $SrGd_{1.7}(MoO_4)_4:Er_{0.1}Yb_{0.2}$ and (d) $SrGd_{1.5}(MoO_4)_4:Er_{0.05}Yb_{0.45}$ particles excited under 980 nm at room temperature

For Er^{3+}/Yb^{3+} co-doped upconversion phosphors, the Yb^{3+} ion sensitizer can be effectively excited by the energy of the incident light source, which transfers this energy to the activator, where radiation can be emitted. The Er^{3+} ion activator is the luminescence center in upconversion particles and the sensitizer enhances the upconversion luminescence efficiency due to the energy matching of the gap between the $^2F_{7/2}$ and the $^2F_{5/2}$ of Yb^{3+}. Fig. 5 shows the schematic energy level diagrams of Er^{3+} ions (activator) and Yb^{3+} ions (sensitizer) in the as-prepared $SrGd_2(MoO_4)_4:Er^{3+}/Yb^{3+}$ samples and the upconversion mechanisms accounting for the green and red emissions at 980 nm laser excitation. The upconversion emissions are generated through multiple processes of ground state absorption (GSA) and energy transfer (ET). For the green emissions, under the excitation of 980 nm, the Yb^{3+} ion sensitizer is excited from the ground state of the $^2F_{7/2}$ to the excited state of the $^2F_{5/2}$ through ground state absorption process and transfers the energy to the excited Er^{3+} ions and promotes it from the $^4I_{15/2}$ to the $^4I_{11/2}$ by the energy transfer process of $^4I_{15/2}$ (Er^{3+}) + $^2F_{5/2}$ $(Yb^{3+}) \rightarrow {}^4I_{11/2}$ (Er^{3+}) + $^2F_{7/2}$ (Yb^{3+}). Another Yb^{3+} ion at the $^2F_{5/2}$ level transfers the energy to the excited Er^{3+} ion and then transits further the energy from the $^4I_{11/2}$ to the higher $^4F_{7/2}$ level by another energy transfer process of $^4I_{11/2}$ (Er^{3+}) + $^2F_{5/2}$ $(Yb^{3+}) \rightarrow {}^4F_{7/2}$ (Er^{3+}) + $^4F_{7/2}$ (Yb^{3+}), which are for the population of the different level in Er^{3+}. The populated $^4F_{7/2}$ level relaxes rapidly and non-radiatively to the next lower $^2H_{11/2}$ and $^4S_{3/2}$ in Er^{3+} because of the short lifetime of the $^4F_{7/2}$ level. Then, the radiative transitions of $^2H_{11/2} \rightarrow {}^4I_{15/2}$ and $^4S_{3/2} \rightarrow {}^4I_{15/2}$ processes can produce green emission at 525 and 550 nm. It is noted that the green upconversion luminescence can be induced by a two-photon process[10,28]. For the red emission, the $^4F_{9/2}$ level is populated by non-radiative relaxation from the $^4S_{3/2}$ to the $^4F_{9/2}$ level and the second energy transfer from the $^4I_{13/2}$ to the $^4F_{9/2}$ level in Er^{3+}. Finally, the $^4F_{9/2}$ level relaxes radiatively to the ground state at the $^4I_{15/2}$ level and releases red emission at 655 nm[29]. The strong 525 and 550 nm emission bands in the green region as shown in Fig. 4 are assigned to the $^2H_{11/2} \rightarrow {}^4I_{15/2}$ and $^4S_{3/2} \rightarrow {}^4I_{15/2}$ transitions of Er^{3+} ions, respectively, while the weak 655-nm emission band in the red region is assigned to the $^4F_{9/2} \rightarrow {}^4I_{15/2}$ transition. The much higher intensity of the $^2H_{11/2} \rightarrow {}^4I_{15/2}$ transition in comparison with that of the $^4S_{3/2} \rightarrow {}^4I_{15/2}$ transition in Fig. 4 may be induced with the concentration quenching effect by the energy transfer between the nearest Er^{3+} and Yb^{3+} ions and the interactions between doping ions in the $SrGd_2(MoO_4)_4$ host matrix[7,29]. It means that the green band $^2H_{11/2} \rightarrow {}^4I_{15/2}$ transitions are assumed to be more easily quenched than that of the $^4S_{3/2} \rightarrow {}^4I_{15/2}$ transition by the non-radiative relaxation in the case of $SrGd_2(MoO_4)_4$ host matrix.

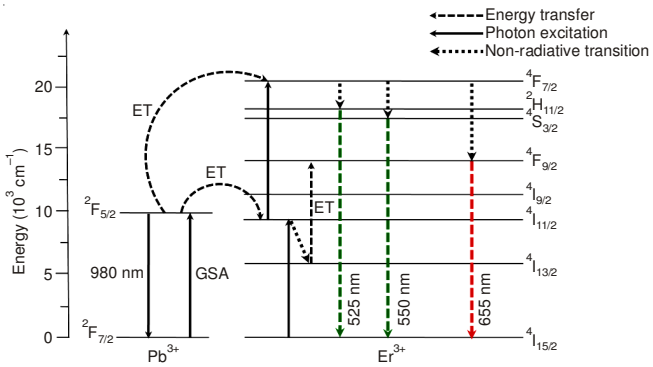

Fig. 5. Schematic energy level diagrams of Er^{3+} ions (activator) and Yb^{3+} ions (sensitizer) in the as-prepared $SrGd_2(MoO_4)_4:Er^{3+}/Yb^{3+}$ system and the upconversion mechanisms accounting for the green and red emissions under 980 nm laser excitation

Fig. 6 shows the Raman spectra of the synthesized (a) $SrGd_2(MoO_4)_4$ (SGM), (b) $SrGd_{1.8}(MoO_4)_4:Er_{0.2}$ (SGM:Er), (c) $SrGd_{1.7}(MoO_4)_4:Er_{0.1}Yb_{0.2}$ (SGM:ErYb) and (d) $SrGd_{1.5}(MoO_4)_4:Er_{0.05}Yb_{0.45}$ (SGM:ErYb#) particles excited by the 514.5 nm line of an Ar ion laser at 0.5 mW on the samples. The internal modes for the (a) $SrGd_2(MoO_4)_4$ (SGM) particles were detected at 323, 338, 772 and 903 cm^{-1}, respectively. The well-resolved sharp peaks for the $SrGd_2(MoO_4)_4$ particles indicate the high crystallization state of the synthesized particles. The internal vibration mode frequencies are dependent on the lattice parameters and the degree of the partially covalent bond between the cation and molecular ionic group $[MoO_4]^{2-}$. The Raman spectra of the (b) $SrGd_{1.8}(MoO_4)_4:Er_{0.2}$ (SGM:Er), (c) $SrGd_{1.7}(MoO_4)_4:Er_{0.1}Yb_{0.2}$ (SGM:ErYb) and (d) $SrGd_{1.5}(MoO_4)4:Er_{0.05}Yb_{0.45}$ (SGM:ErYb#) particles indicate the domination of strong peaks at higher frequencies (1023, 1092 and 1325 cm^{-1}) and at lower frequencies (233, 293, 365, 428, 538 and 594 cm^{-1}).

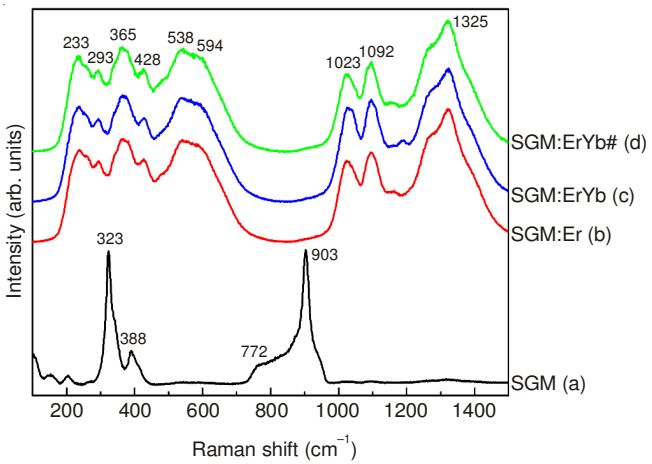

Fig. 6. Raman spectra of the synthesized (a) $SrGd_2(MoO_4)_4$ (SGM), (b) $SrGd_{1.8}(MoO_4)_4:Er_{0.2}$ (SGM:Er), (c) $SrGd_{1.7}(MoO_4)_4:Er_{0.1}Yb_{0.2}$ (SGM:ErYb) and (d) $SrGd_{1.5}(MoO_4)_4:Er_{0.05}Yb_{0.45}$ (SGM:ErYb#) particles excited by the 514.5 nm line of an Ar ion laser at 0.5 mW on the samples

Conclusion

The $SrGd_2(MoO_4)_4:Er^{3+}/Yb^{3+}$ green phosphors with doping concentrations of Er^{3+} and Yb^{3+} were successfully synthesized by a cyclic microwave-assisted sol-gel method and the upconversion mechanisms were investigated. Well-crystallized particles, formed after heat-treatment at 900 °C for 12 h, showed a fine and homogeneous morphology with particle sizes of 2-5 μm. Under excitation at 980 nm, $SrGd_{1.7}(MoO_4)_4$-:$Er_{0.1}Yb_{0.2}$ and $SrGd_{1.5}(MoO_4)_4:Er_{0.05}Yb_{0.45}$ particles exhibited strong 525 and 550 nm emission bands in the green region, which were assigned to the $^2H_{11/2} \rightarrow {}^4I_{15/2}$ and $^4S_{3/2} \rightarrow {}^4I_{15/2}$ transitions, respectively, while a weak 655 nm emission band in the red region was assigned to the $^4F_{9/2} \rightarrow {}^4I_{15/2}$

transition by a two-photon process. The upconversion intensity of $SrGd_{1.5}(Mo\text{-}O_4)_4:Er_{0.05}Yb_{0.45}$ particles was much higher than that of the $SrGd_{1.7}(MoO_4)_4:Er_{0.1}Yb_{0.2}$ particles. The Raman spectra of $SrGd_{1.8}(MoO_4)_4:Er_{0.2}$, $SrGd_{1.7}(MoO_4)_4:Er_{0.1}Yb_{0.2}$ and $SrGd_{1.5}(MoO_4)_4:Er_{0.05}Yb_{0.45}$ particles indicated the domination of strong peaks at higher frequencies (1023, 1092 and 1325 cm^{-1}) and at lower frequencies (233, 293, 365, 428, 538 and 594 cm^{-1}).

ACKNOWLEDGEMENTS

This study was supported by the Basic Science Research Program through the National Research Foundation of Korea (NRF) funded by the Ministry of Science, ICT & Future Planning (2014-046024).

REFERENCES

1. Y.J. Chen, H.M. Zhu, Y.F. Lin, X.H. Gong, Z.D. Luo and Y.D. Huang, *Opt. Mater*., **35**, 1422 (2013).
2. M. Wang, G. Abbineni, A. Clevenger, C. Mao and S. Xu, *Nanomedicine*, **7**, 710 (2011).
3. C. Zhang, L. Sun, Y. Zhang and C. Yan, *J. Rare Earths*, **28**, 807 (2010).
4. C. Guo, H.K. Yang and J.H. Jeong, *J. Lumin*., **130**, 1390 (2010).
5. J. Sun, Y. Lan, Z. Xia and H. Du, *Opt. Mater.*, **33**, 576 (2011).
6. J. Liao, D. Zhou, B. Yang, R. Liu, Q. Zhang and Q. Zhou, *J. Lumin*., **134**, 533 (2013).
7. J. Sun, J. Xian and H. Du, *J. Phys. Chem. Solids*, **72**, 207 (2011).
8. V.K. Komarala, Y. Wang and M. Xiao, *Chem. Phys. Lett*., **490**, 189 (2010).
9. J. Sun, J. Xian, Z. Xia and H. Du, *J. Rare Earths*, **28**, 219 (2010).
10. H. Du, Y. Lan, Z. Xia and J. Sun, *Mater. Res. Bull*., **44**, 1660 (2009).
11. L.X. Pang, H. Liu, D. Zhou, G.B. Sun, W.B. Qin and W.G. Liu, *Mater. Lett*., **72**, 128 (2012).
12. M. Haque and D.K. Kim, *Mater. Lett*., **63**, 793 (2009).
13. C. Zhao, X. Yin, F. Huang and Y. Hang, *J. Solid State Chem*., **184**, 3190 (2011).
14. L. Qin, Y. Huang, T. Tsuboi and H.J. Seo, *Mater. Res. Bull*., **47**, 4498 (2012).
15. Y. Yang, E. Liu, L. Li, Z. Huang, H. Shen and X.- Xiang, *J. Alloys Comp*., **505**, 555 (2010).
16. Y. Tian, B. Chen, B. Tian, R. Hua, J. Sun, L. Cheng, H. Zhong, X. Li, J. Zhang, Y. Zheng, T. Yu, L. Huang and Q. Meng, *J. Alloys Comp*., **509**, 6096 (2011).
17. Y. Huang, L. Zhou, L. Yang and Z. Tang, *Opt. Mater*., **33**, 777 (2011).
18. Y. Tian, B. Chen, B. Tian, J. Sun, X. Li, J. Zhang, L. Cheng, H. Zhong, H. Zhong, Q. Meng and R. Hua, *Physica B*, **407**, 2556 (2012).
19. Z. Wang, H. Liang, L. Zhou, J. Wang, M. Gong and Q. Su, *J. Lumin*., **128**, 147 (2008).
20. Q. Chen, L. Qin, Z. Feng, R. Ge, X. Zhao and H. Xu, *J. Rare Earths*, **29**, 843 (2011).
21. X. Shen, L. Li, F. He, X. Meng and F. Song, *Mater. Chem. Phys*., **132**, 471 (2012).
22. J. Zhang, X. Wang, X. Zhang, X. Zhao, X. Liu and L. Peng, *Inorg. Chem. Commun*., **14**, 1723 (2011).
23. C.S. Lim, *Mater. Chem. Phys*., **131**, 714 (2012).
24. C.S. Lim, *J. Lumin*., **132**, 1774 (2012).
25. J.C. Sczancoski, L.S. Cavalcante, M.R. Joya, J.A. Varela, P.S. Pizani and E. Longo, *Chem. Eng. J*., **140**, 632 (2008).
26. C.S. Lim, *Mater. Res. Bull*., **48**, 3805 (2013).
27. W. Lu, L. Cheng, J. Sun, H. Zhong, X. Li, Y. Tian, J. Wan, Y. Zheng, L. Huang, T. Yu, H. Yu and B. Chen, *Physica B*, **405**, 3284 (2010).
28. J. Sun, J. Xian, X. Zhang and H. Du, *J. Rare Earths*, **29**, 32 (2011).
29. Q. Sun, X. Chen, Z. Liu, F. Wang, Z. Jiang and C. Wang, *J. Alloys Comp*., **509**, 5336 (2011).